ACS APPLIED MATERIALS & INTERFACES

Research Article

www.acsami.org

Facile Synthesis of Porous Metal Oxide Nanotubes and Modified Nafion Composite Membranes for Polymer Electrolyte Fuel Cells Operated under Low Relative Humidity

Kriangsak Ketpang, Kibong Lee, and Sangaraju Shanmugam*

Department of Energy Systems Engineering, Daegu Gyeongbuk Institute of Science & Technology (DGIST) 50-1, Sang-Ri, Hyeonpung-Myeon, Dalseong-Gun, Daegu, Republic of Korea, 711-873

Supporting Information

ABSTRACT: We describe a facile route to fabricate mesoporous metal oxide (TiO_2, CeO_2 and $ZrO_{1.95}$) nanotubes for efficient water retention and migration in a Nafion membrane operated in polymer electrolyte fuel cell under low relative humidity (RH). Porous TiO_2 nanotubes (TNT), CeO_2 nanotubes (CeNT), and $ZrO_{1.95}$ (ZrNT) were synthesized by calcining electrospun polyacrylonitrile nanofibers embedded with metal precursors. The nanofibers were prepared using a conventional single spinneret electrospinning technique under an ambient atmosphere. Their porous tubular morphology was observed by SEM and TEM analyses. HR-TEM results revealed a porous metal oxide wall composed of small particles joined together. The mesoporous structure of the samples was analyzed using BET. The tubular morphology and outstanding water absorption ability of the TNT, CeNT, and ZrNT fillers resulted in the effective enhancement of proton conductivity of Nafion composite membranes under both fully humid and dry conditions. Compared to a commercial membrane (Nafion, NRE-212) operated under 100% RH at 80 °C, the Nafion−TNT composite membrane delivered approximately 1.29 times higher current density at 0.6 V. Compared to the Nafion-TiO_2 nanoparticles membrane, the Nafion−TNT membrane also generated higher current density at 0.6 V. Additionally, compared to a NRE-212 membrane operated under 50% RH at 80 °C, the Nafion−TNT composite membrane exhibited 3.48 times higher current density at 0.6 V. Under dry conditions (18% RH at 80 °C), the Nafion−TNT, Nafion-CeNT, and Nafion-ZrNT composite membranes exhibited 3.4, 2.4, and 2.9 times higher maximum power density, respectively, than the NRE-212 membrane. The remarkably high performance of the Nafion composite membrane was mainly attributed to the reduction of ohmic resistance by the mesoporous hygroscopic metal oxide nanotubes, which can retain water and effectively enhance water diffusion through the membrane.

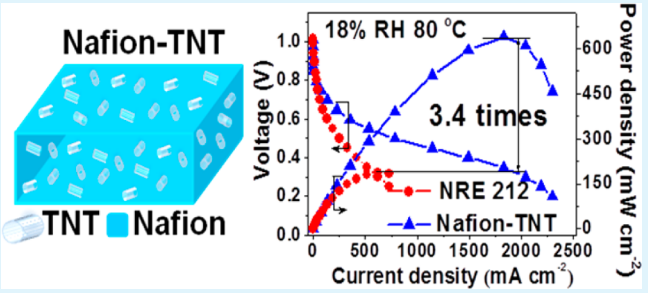

KEYWORDS: *Nafion composite membrane, mesoporous TiO_2 nanotubes, metal oxide, PEFCs, electrospinning*

INTRODUCTION

Recent research in polymer electrolyte fuel cells (PEFCs) operated under low relative humidity (RH) has focused on simplifying thermal management and reducing the cost of the system.[1] However, the current PEFC technology, which utilizes perfluorosulfonic acid (PFSA) polymer membranes, for example, Nafion, as an electrolyte, exhibits poor performance under low RH.[1] The deterioration of PEFCs performance under this condition is mainly due to the loss of proton conductivity of the Nafion membrane, which results in a drastic increase of ohmic overpotential.[2] The proton conductivity of Nafion membrane is highly influenced by the amount of water present in the membrane, and the proton conductivity is maximal when the membrane is fully saturated with water.[3,4] Operating PEFCs under low RH leads to membrane dehydration, which remarkably reduces the proton conductivity.[4] It is thus highly desirable to enhance the proton conductivity of the Nafion membrane under low RH so as to achieve higher PEFCs performance.

An effective approach to improve the proton conductivity of Nafion membranes under low RH is to incorporate bifunctional ceramic/inorganic fillers in the membrane, such as SiO_2,[5−12] TiO_2,[11−25] ZrO_2,[11−13,26,27] heteropolyacids,[28] and zeolites,[29] etc., which are both hygroscopic and proton conductors. Hygroscopic inorganic fillers contain water in the molecular framework which does not evaporate even at a temperature greater than 100 °C because of electrostatic attraction within the electrical double layer (EDL).[19] The insolubility of these compounds in aqueous media also prevents them leaching out from the membrane.[19] Nevertheless, incorporating hygroscopic nanoparticle fillers in Nafion membrane does not enhance fuel

Received: June 16, 2014
Accepted: September 9, 2014
Published: September 9, 2014

 © 2014 American Chemical Society

cell performance operated under fully humid conditions because there is insufficient water-back diffusion from cathode to anode.[11−13,15,16,19] Generally, water provided from an external humidification system delivers protons through the membrane from anode to cathode electrodes. At the same time, water is also produced at the cathode electrode by oxygen reduction reaction. Thus, a large amount of water located at the cathode electrode must be removed, otherwise the oxidant cannot reach the active sites of the cathode catalyst layer.[14] In addition, as more oxidant reaches the cathode active catalyst layer, it will have the effect of suppressing the mass transport overpotential.[14] Thus, incorporating a porous hygroscopic filler with tubular morphology into a Nafion membrane could be an effective approach to enhance the performance of Nafion membranes operated under fully humid and low RH conditions.[16,17] This is because the tubular hygroscopic filler can not only provide water retention capability but also effectively enhance the water diffusion (water electroosmotic and water back diffusion) in a Nafion membrane.[16,17] That incremental water retention ability and efficient water diffusion should be capable of suppressing the ohmic resistance of the membrane as well as increasing cathode catalyst utilization.[14,16,17]

Among the tubular hygroscopic fillers, titanium dioxide nanotubes (TNT) are conventionally prepared by chemical and electrochemical methods using various hazardous bases and acids.[30,31] To avoid the use of hazardous chemicals, electrospinning and emulsion electrospinning techniques have been employed to fabricate porous TNT.[32,33] However, TNT prepared using a coaxial electrospinning technique requires a specially designed dual capillary nozzle, and the oil contained in the fibers must be removed using an organic solvent to form a hollow structure.[32] On the other hand, high temperature (90 °C) must be maintained during the preparation of TNT using emulsion electrospinning to keep moisture out during electrospining.[33] Furthermore, the diameter of the TNT fabricated by both coaxial and emulsion electrospinning methods are relatively large, which leads to low surface area.[32,33] Thus, developing a process for synthesizing porous TNT with diameters smaller than 100 nm using a conventional single spinneret electrospinning technique is a key challenge that must be surmounted to obtain high surface area TNT, which could then be beneficially employed to enhance water retention and diffusion in Nafion membrane.

In this study, we report a simple and straightforward method to synthesize porous metal oxide nanotubes with diameter smaller than 100 nm. This was achieved by calcination of an electrospun polyacrylonitrile (PAN) containing a metal precursor mat prepared using conventional single spinneret electrospinning, under an air atmosphere. This synthetic route is relatively simple, is cost-effective, and is performed under mild synthesis conditions without any hazardous chemicals. The yield of synthesized metal oxide was around 95−99% based on the precursor. The novelty of this study lies in the synthesis of TNT and zirconium dioxide nanotubes (ZrNT) with diameters smaller than 100 nm using a conventional single spinneret electrospinning technique, which has not been reported to date. The fabricated porous metal oxide nanotubes were incorporated in a Nafion ionomer and subsequently a PEFC performance was further evaluated for the prepared composite membranes under 18%, 50%, and 100% RH at 80 °C. The PEFC results using the composite membranes were compared with those obtained using commercial NRE-212 and recast Nafion membranes.

EXPERIMENTAL SECTION

Materials. Polyacrylonitrile (PAN, M_w = 150 000 g/mol), titanium(IV) oxyacetylacetonate (TiOacac), cerium(III) acetylacetonate (Ceacac), and zirconium(IV) acetylacetonate (Zracac) were purchased from Aldrich, Korea. Nafion ionomer (1100 EW, 15 wt %) was purchased from Ion Pow. Inc., USA. Nafion 212 (NRE-212) membrane was purchased from Aldrich, Korea. *N*,*N*-dimethylformamide (DMF), ethanol, H_2O_2, H_2SO_4, and isopropyl alcohol (IPA) were purchased from Daejung Chemicals, Korea, and were used as received.

Preparation of Electrospun (E-Spun) Composites Nonwoven Web. TiOacac (0.1 g) or Zracac (0.1 g) or Ceacac (0.2 g) was completely dissolved in 3.00 g of DMF at 90 °C. PAN (1 g) was also completely dissolved in DMF 6.00 g at 90 °C. Then, the Macac precursor solution and PAN solution was mixed and stirred at 90 °C until a clear homogeneous solution was observed. The electrospinning process is described elsewhere.[34] The solution was electrospun using electrospinning set up (NanoNC.ltd) under conditions: traveling distance between spinneret to collector of 10 cm, high voltage power supply of 15 kV, volume feed rate of 1.0 mL h^{-1} and rotating speed of 300 rpm, respectively under humidity <30% RH at 20−25 °C.

Preparation of Porous Metal Oxide Nanotubes. TNT was prepared by calcining the as-spun PAN/TiOacac composite nonwoven web in a tubular furnace (Wisd Laboratory Instruments) at 600 °C for 3 h. The calcination process was carried out under air atmosphere in which the composite nonwoven web was stabilized at 250 °C for 1 h to remove an organic materials and then heating to 600 °C for 3 h. The heating rate was fixed at 5 °C per minute. ZrNT and cerium dioxide nanotubes (CeNT) were prepared using a similar approach but with a different calcination temperature ZrNT (600 °C, 1 h) and CeNT (500 °C, 1 h) was used.

Preparation of Nafion−Metal Oxide Nanotube Composite Membrane. TNT, ZrNT, and CeNT with different mass ratios were incorporated in Nafion ionomer using ethanol as solvent and the mixture solution was then ultrasonicated for 60 min followed by mechanical stirring for 6 h. The composite membranes were prepared by casting these solutions on a glass Petri dish and allowed to dry at 50 °C for 2 h, 60 °C for 2 h, 70 °C for 2 h, and 80 °C for 2 h using vacuum oven. The composite membranes were peeled off by utilization of DI water. For comparison, Nafion ionomer was cast in a similar manner without any filler materials. The dry membrane thickness of all composite membranes was measured at 5 random points over the surface using a digital micrometer and the average thickness was found to be ∼50 ± 5 μm. Finally, the membranes were pretreated by boiling in 5% H_2O_2, H_2O, 0.5 M H_2SO_4, and H_2O in sequence for 1 h in each case.

Materials Characterizations. The morphology of the samples was observed using a field-emission scanning electron microscope (FE-SEM, Hitachi, S-4800 II) with an accelerating voltage of 3 kV. Before the observation, the samples were coated with osmium. The microstructures and lattice fringe of samples were determined by field-emission transmission electron microscope (FE-TEM, Hitachi, HF-3300) with an acceleration voltage of 300 kV. For TEM analysis, samples were ultrasonically dispersed in ethanol, and then a drop of dispersion was deposited on copper grid and dry under UV lamp.

The crystal structure of calcined samples was investigated by powder X-ray diffraction (XRD, Panalytical, Empyrean) using Cu K-alpha radiation at a generator voltage of 40 kV and a tube current of 30 mA.

The pore structure and surface area of samples was determined by the N_2 adsorption/desorption isotherm analysis using Micromeritics ASAP 2000 surface area and porosity analyzer. The samples were degassed at 150 °C for 6 h before analysis.

Water uptake (WU) of samples was determined by drying membranes in the oven at 90 °C overnight and the membranes

were then soaked in DI water for 24 h at room temperature. WU was calculated by the following eq 1

$$\mathrm{WU}(\%) = \frac{W_{\mathrm{swollen}} - W_{\mathrm{dry}}}{W_{\mathrm{dry}}} \times 100 \quad (1)$$

where W_{swollen} is the weight of the membrane that was soaked in water for 24 h and W_{dry} is the weight of dry membrane.

Ion exchange capacity (IEC) was investigated by an acid−base titration using phenolphthalein as an indicator. The samples were dried in the oven at 90 °C overnight and the membranes were then immersed in 3.0 M NaCl solution for 12 h so that the H^+ of membrane could be exchanged with Na^+. The solution was finally titrated with 0.01 M NaOH. IEC value was calculated according to eq 2

$$\mathrm{IEC} = \frac{V_{\mathrm{NaOH}} \times C_{\mathrm{NaOH}}}{W_{\mathrm{dry}}} \quad (2)$$

where IEC was the ion exchange capacity (mequiv g^{-1}), V_{NaOH} was the added volume of NaOH at the equivalent point (mL), C_{NaOH} was the concentration of NaOH (M), and W_{dry} is the weight of dry membrane.

The number of water molecule per sulfonic acid group, λ, was calculated by following eq 3[35]

$$\lambda = \frac{\mathrm{WU}\ (\%) \times 10}{18 \times \mathrm{IEC}\ (\mathrm{mmol\ g^{-1}})} \quad (3)$$

The amount of bound water present in membranes was estimated using differential scanning colorimeter (DSC, TA Instruments). In DSC experiment, the swollen membranes were frozen at −80 °C and held for 5 min. After that, the membranes were heated to 80 °C with a heating rate of 1 °C min^{-1}. The amount of nonfreezing bound water in the hydrated membrane was determined following eq 4

$$W_{\mathrm{b}}(\%) = \mathrm{WU} - (W_{\mathrm{f}} + W_{\mathrm{fb}}) = \mathrm{WU} - \left(\frac{Q_{\mathrm{endo}}}{Q_{\mathrm{pure}}} \times 100\right) \quad (4)$$

where W_{b} was the amount of nonfreezing bound water (%) and WU was the water uptake, W_{f} and W_{fb} were the amounts of free water and freezable loosely bound water, respectively. Q_{endo} was the endothermic fusion enthalpy of fully hydrated membrane (freezable loosely bound water and free water) calculated by DSC (J g^{-1}) and Q_{pure} was the enthalpy of deionized water (334 J g^{-1}).[36]

The proton conductivity of the membranes was measured in the longitudinal direction with a four-probe method using membrane conductivity cell (Bekktech) with gas flowing options. Membrane samples with area of 0.7 cm × 3.0 cm were assembled in the cell, in contact with two platinum electrodes placed at a fixed position. The potentiostat is set to apply specific voltages between two Pt electrodes and resulting currents were measured. The resistance (R) is derived from the slope of the line that connects the data points. The membrane conductivity as a function of relative humidity percentages (RH %) at 80 °C was determined according to eq 5

$$\sigma = \frac{L}{R \times W \times T} \quad (5)$$

where L = 0.425 cm is the fixed distance between two Pt electrodes, R is the membrane resistance in Ω, W is the width of the sample in centimeters, and T is the thickness of the membrane in centimeters.

Fabrication of Membrane Electrode Assemblies and Fuel Cell Performance Evaluation. The PEFC performance of membranes was evaluated by making membrane electrode assemblies (MEAs). Diffusion-layer coated carbon papers (SGL, thickness = 0.27 mm) were used as the backing layers. For the catalyst layer, 40 wt % Pt/C catalyst (Johnson Matthey) was first mixed with DI water and 30 wt % Nafion solution (5% Nafion ionomer) followed by isopropyl alcohol. The resultant slurry was ultrasonicated for 60 min and it was represented as cathode catalyst. For anode catalyst layer, 40 wt % Pt/C was prepared a similar manner to cathode reaction layer but the concentration of Nafion ionomer was 7 wt %. Catalyst was coated on backing layers with loading of 1.0 mg cm^{-2} for both the anode and cathode. The active area for the PEFCs was 5 cm^2. A thin layer of Nafion ionomer was applied to the catalyst surface of both the electrodes. MEAs were obtained by sandwiching the membrane between the cathode and anode followed by its hot-compaction under a pressure of 20 kg cm^{-2} at 130 °C for 2 min. MEAs were coupled with Teflon gas-sealing gaskets and placed in single-cell test fixtures with parallel serpentine flow-field machined on graphite plates. Before conducting the polarization plots, the MEAs were stabilized at 0.6 V for 6 h under each RH condition (18%, 50%, and 100% RH) by passing hydrogen and oxygen gases which were heated at a required temperature to anode and cathode sides, respectively,. The flow rate of hydrogen and oxygen gases was fixed at 300 sccm through a mass flow controller and the cell temperature was fixed at 80 °C. The polarization data are collected point by point and 1 min is given to the system to come to steady state. The reproducibility of the data was ascertained by repeating the experiments at least twice. All the MEAs were evaluated in PEFCs under atmospheric pressure without back pressure.

RESULTS AND DISCUSSION

Characterization of Porous Metal Oxide Nanotubes. The porous TNT was fabricated by a two-step process. Electrospun fibers containing titanium precursor were first prepared using a single spinneret electrospinning technique under ambient conditions. The electrospinning technique was used to fabricate a fiber template in which the titanium precursor was finely dispersed. However, fiber was not formed when only the precursor solution was spun, owing to its low viscosity. PAN was thus incorporated to increase the precursor solution viscosity. An as-spun mat of light yellow color was obtained on a piece of Al foil. After that, the as-spun mats were thermally stabilized at 250 °C for 1 h and then the stabilized mats were pyrolyzed at 600 °C for 3 h under an air atmosphere. The calcined samples are hereafter denoted as TNT.

Figure 1a displays the X-ray diffraction (XRD) patterns of the TNT sample. The as-prepared sample was a mixture of

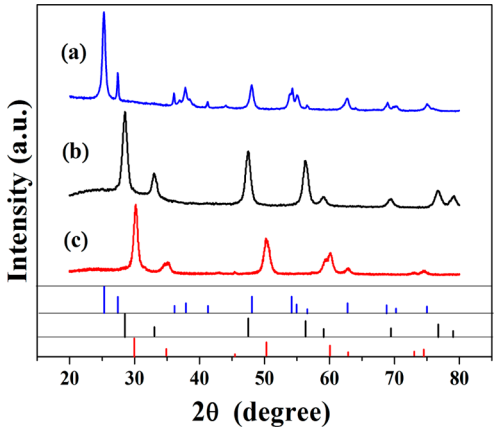

Figure 1. Powder X-ray diffraction pattern of samples TNT (a), CeNT (b), and ZrNT (c).

anatase and rutile phase TiO_2. The amount of anatase and rutile phases detected from XRD was around 75% and 25%, respectively. Figure 2a shows the morphology of the TNT sample. The SEM image indicates a tubular morphology with various lengths of nanotubes. The average outer diameter of the TNTs was found to be 50 nm (Supporting Information Figure S1a). The inner diameter of a TNT was in the range of 10−50 nm. A transmission electron microscope (TEM) was used to observe the microstructure of the TNT. The TEM image

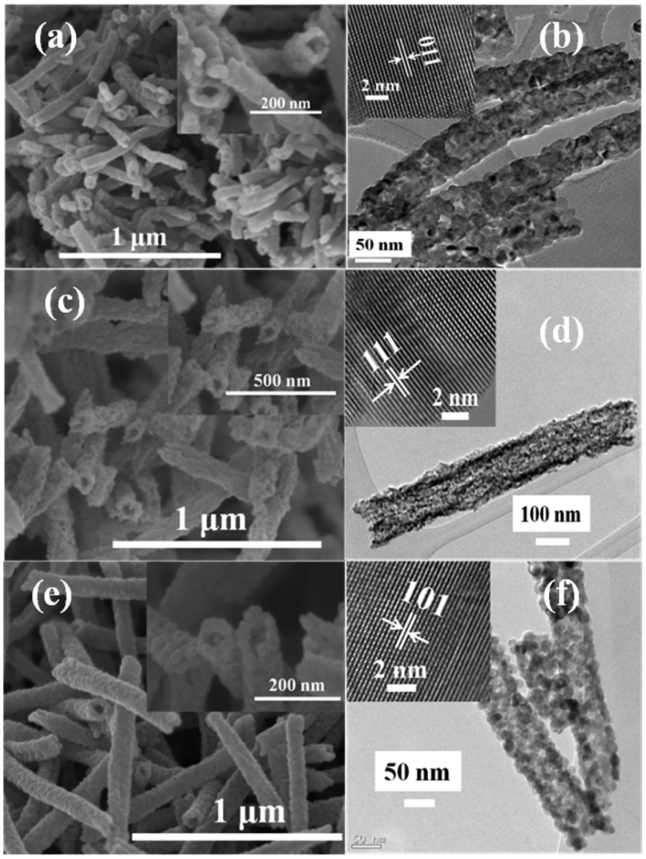

Figure 2. FE-SEM images of samples TNT (a), CeNT (c), ZrNT (e), TEM images and corresponding lattice fringes (inset) of sample TNT (b), CeNT (d), and ZrNT (f).

clearly shows the existence of porous nanotubes, where the tube wall consists of small particles joined together, (Figure 2b). The nanotube wall thickness was observed to be 8 nm. The high resolution TEM images show lattice fringes with an interplanar distance of 0.35 nm (inset of Figure 2b), corresponding to the (011) plane of anatase TiO_2. To determine the pore structure and specific surface area, TNT sample was analyzed by N_2 adsorption−desorption isotherms and the results are illustrated in Figure 3 (a, b). According to IUPAC classification, the sorption isotherm of TNT was type IV and the hysteresis loop was of type H3 (Figure 3 a).[37,38] The N_2 sorption isotherm results show that the synthesized TNT was a mesoporous material with mainly cylindrical pore shape.[37] In addition, the type H3 hysteresis loop was indicative of an aggregation of joined particles giving rise to slit-shaped pores.[37] The sorption isotherm and pore size distribution results highly supported the porous morphology observed by TEM analysis. The BET surface area and average pore diameter of the TNT samples were found to be 35.39 $m^2\ g^{-1}$ and 15 nm, respectively (Table 1).

The developed methodology was extended to prepare other metal (Ce, and Zr) oxide nanotubes. Figure 1 (b and c) depicts the XRD patterns of prepared CeNT and ZrNT and patterns of the CeNT and ZrNT samples were perfectly matched to CeO_2 (Figure 1b) and $ZrO_{1.95}$ (Figure 1c). Figures 2 c and e shows the SEM images of the CeNT and ZrNT samples, exhibiting tubular morphology. The average outer diameter of CeNTs and ZrNTs was found to be 113 and 90 nm, (Supporting Information Figure S1b and c), while their inner diameter was in the range of 30−70 and 20−40 nm, respectively. Figure 2d and f illustrates the microstructure of the CeNT and ZrNT samples observed by TEM. Both samples show that small particles have aggregated, forming a tubular structure. The tube wall thickness of the CeNT and ZrNT corresponds to 8.5 and 9 nm, respectively. The high resolution TEM images of CeNT and ZrNT show lattice fringes with an interplanar distance of 0.295 and 0.311 nm (inset of Figure 2d and f, corresponding to the (111) plane of CeO_2 and (101) plane of $ZrO_{1.95}$. Figure 3c−f displays the N_2 adsorption−desorption isotherms of the CeNT and ZrNT samples. It was found that the CeNT and ZrNT exhibit type IV N_2 sorption isotherms, and the hysteresis loop at high P/P_0 can be attributed to type H3, which implies a mesoporous structure formed by the aggregation of small particles joined together. The BET surface area of the CeNT and ZrNT was 27.84 and 51.19 $m^2\ g^{-1}$, respectively (Table 1) and the pore diameter of the CeNT and ZrNT was found to be 15 and 10 nm, respectively.

The mechanism underlying the formation of metal oxide nanotubes by this method is yet to be elucidated. It can be presumed that the metal precursor was homogeneously dispersed in the electrospun fibers during the electrospinning process. In the calcinations process, metal ions on the fiber surface interacted with ambient air, forming metal oxide clusters on the fiber surface at a temperature of 400 °C. These metal oxide clusters aggregated together along the fiber template forming a rigid shell, however, the polymeric carbon did not completely decompose yet at this temperature. Upon reaching a temperature of 600 °C, the carbon would be completely decomposed, leaving a hollow structure.[39]

Characterization of Composite Membranes. Subsequently, the as-produced TNT was utilized as filler in composite membranes and then incorporated in a Nafion ionomer to provide the water retention capability in the Nafion membrane. Proton conductivity is an important property which directly influences the performance of an electrolyte membrane. Higher proton conductivity value of membrane results in better PEFC performance. Therefore, the proton conductivity of various Nafion−TNT composite membranes was evaluated and the obtained results were compared with the NRE-212 and recast Nafion membranes at 80 °C under different level of humidity. The Nafion−TNT composite membranes with TNT filler contents of 1.0, 1.5, and 2.0 wt % were denoted as Nafion−TNT-1.0, Nafion−TNT-1.5, and Nafion−TNT-2.0, respectively. Figure 4a compares the proton conductivity of NRE-212, recast Nafion, and Nafion−TNT composite membranes measured at 80 °C under different humidity levels. The proton conductivity under 100% RH at 80 °C of Nafion−TNT-1.0, Nafion−TNT-1.5, and Nafion−TNT-2.0 membranes was 137, 155, and 132 mS cm^{-1}, respectively. The proton conductivity of recast Nafion and NRE-212 membranes was 97 and 103 mS cm^{-1}, respectively. This means that the proton conductivity of Nafion−TNT-1.0, Nafion−TNT-1.5, and Nafion−TNT-2.0 membranes was 1.41, 1.59, and 1.36 times higher than that of the recast Nafion membrane, respectively, and 1.33, 1.50, and 1.28 times higher than that of the NRE-212 membrane. Furthermore, the proton conductivity of the Nafion−TNT composite membrane was also higher than that of the recast Nafion and NRE-212 membranes in all humidity regions. In particular, the proton conductivity of the Nafion−TNT-1.5 composite membrane was 2.07 times higher than that of NRE-212 membrane under 20% RH.

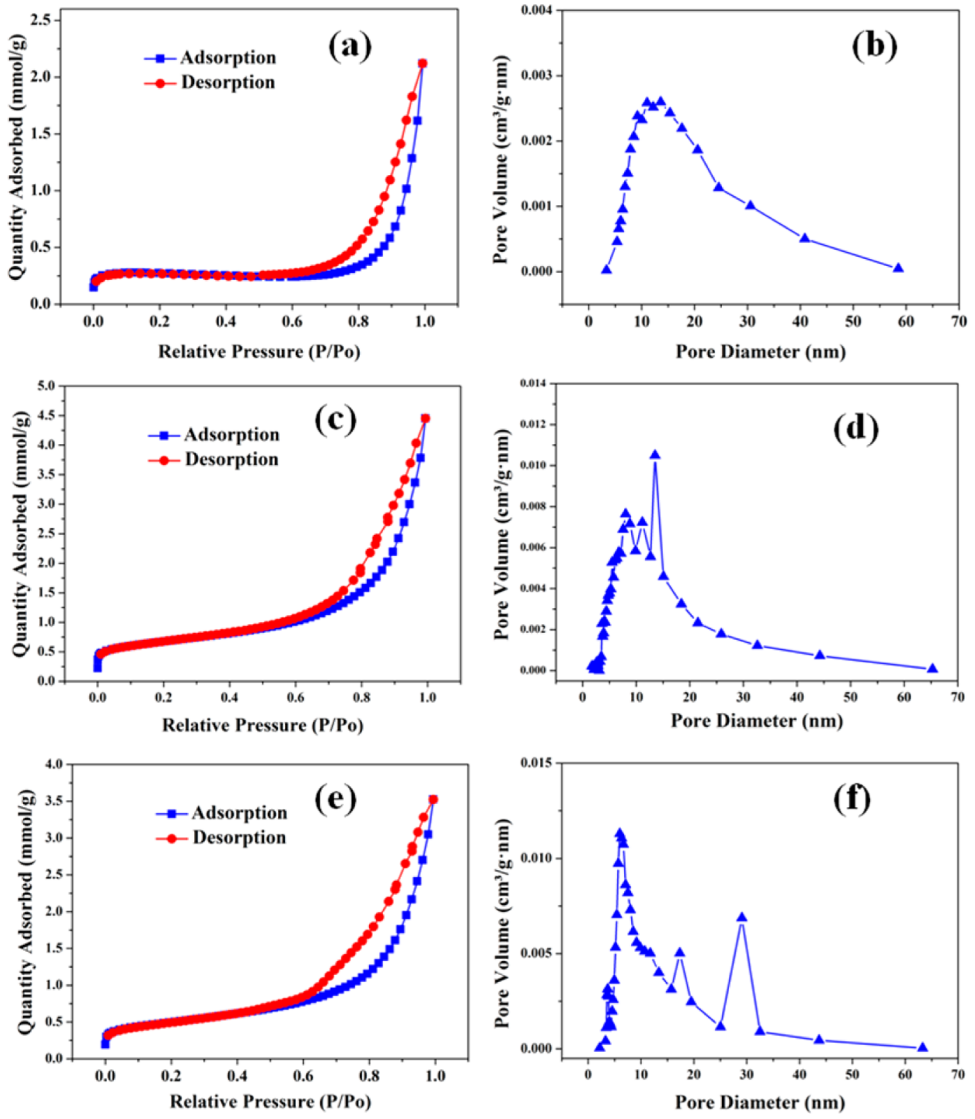

Figure 3. N_2 adsorption−desorption isotherms of TNT (a), CeNT (c), ZrNT (e), and pore-size distribution of TNT (b), CeNT (d), and ZrNT (f).

Table 1. Surface Area and Pore Volume of Synthesized TNT, CeNT, and ZrNT

samples	surface area ($m^2\ g^{-1}$)	BJH desorption cumulative pore volume ($cm^3\ g^{-1}$)
TNT	35.39	0.107
CeNT	27.84	0.099
ZrNT	51.19	0.121

To clarify the remarkably higher proton conductivity of Nafion−TNT composite membranes over the NRE-212 membrane, the state of water of the Nafion−TNT composite membranes was investigated, and the results were compared to results obtained for NRE-212 and recast Nafion membranes. Generally, the proton transport properties of composite membranes highly depend upon the state of water in the membrane, such as free water, freezable loosely bound water and nonfreezing bound water.[36] Freezable loosely bound water is weekly bound to polymer chains, which results in the reduction of phase transition at temperature lower than 0 °C. Free water is not bound to polymer chains and behaves like bulk water. Nonfreezing bound water is strongly bound to the sulfonic acid groups of the polymer chain and plays a major role in the lowering the glass transition temperature. Bound water is responsible for the Grotthuss mechanism by establishing hydrogen bonds between captured water molecules at lower water content in the composite membrane.[4,36] The state of free water, freezable loosely bound water and nonfreezing bound water were investigated using DSC (Supporting Information Figure S2).[36] In this context, the freezable loosely bound water and free water are denoted as freezable water. The state of water distribution in various Nafion−TNT composite membranes in term of freezable water (free water and freezable loosely bound water) and nonfreezing bound water is listed in Table 2. The amount of bound water per mol of sulfonic acid group (λ_{bound}) in Nafion−TNT-1.0, Nafion−TNT-1.5, and Nafion−TNT-2.0 membranes was 7.18, 8.63, and 6.86, respectively. The amount of λ_{bound} in NRE-212 and recast Nafion membranes was 3.60 and 2.61, respectively. In other words, the Nafion−TNT-1.0, Nafion−TNT-1.5, and Nafion−TNT-2.0 membranes exhibited 1.99, 2.39, and 1.9 times higher λ_{bound} than that of NRE-212 and 2.75, 3.31, and 2.62 times higher λ_{bound} than that of recast Nafion membranes. In addition, the Nafion−TNT-1.5 membrane also provided higher freezable water than that of the NRE-212 and recast Nafion membranes.

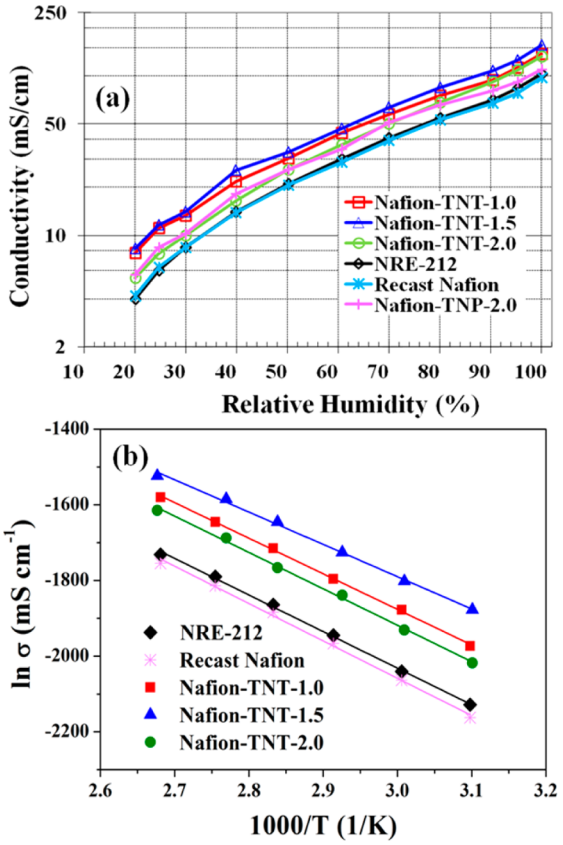

Figure 4. (a) Proton conductivity of NRE-212, recast Nafion, and Nafion−TNT composite membranes measured at 80 °C and (b) regression curves of proton conductivity versus T^{-1} for NRE-212, recast Nafion, and Nafion−TNT composite membranes.

The fact that the Nafion−TNT composite membrane had a higher amount of λ_{bound} than NRE-212 membrane indicates the facile migration of protons through the membrane. To visualize this facile migration of protons in a Nafion−TNT composite membrane, the water self-diffusion coefficients of the Nafion−TNT-1.5 and NRE−212 membranes were determined using the pulsed field gradient nuclear magnetic resonance (PFG NMR) technique on the swelled membranes at a temperature of 25 °C (Supporting Information Figure S3).[27] The water self-diffusion coefficient of the Nafion−TNT-1.5 and NRE-212 membranes was found to be 3.527×10^{-9} and 2.003×10^{-9} m^2 s^{-1}, respectively. The Nafion−TNT membrane exhibited a 1.76 times higher water self-diffusion coefficient than NRE-212 membrane. The remarkably higher water self-diffusion coefficient of Nafion−TNT as compare with NRE-212 membranes indicates that the incorporation of hygroscopic TiO_2 nanotubes effectively not only enhances the water retention capability but also facilitates proton diffusion though the Nafion membrane, yielding higher proton conductivity. On the basis of the proton conductivity results and the data of water states in the membranes, it can be concluded that incorporation of hygroscopic porous tubular TNT can improve water retention ability (free water and bound water in ionic groups of polymer matrix) as well as facilitate water diffusion mobility in the Nafion membrane.[38] However, when the content of TNT filler exceeded 2 wt % it resulted in a lower amount of bound water, which could be due to the aggregation of the TNT filler.[36]

Generally, the proton transport mechanism in a Nafion-based membrane can be either vehicular or Grotthus depending strongly on the amount of water in the membrane.[5] In the vehicular mechanism, the proton combined with water migrates through the membrane, often occurs when the membrane is fully hydrated.[5] On the other hand, in the Grotthus mechanism, the proton hops from one sulfonic acid group to another sulfonic group, and this preferentially happens under low humidity conditions.[5] Both vehicular and Grotthus mechanisms can be identified by evaluating the activation energy of the membrane, which can be determined according to the Arrhenius equation (eq 6)[9,40]

$$\sigma = \sigma_0 e^{-E_a/RT} \tag{6}$$

where σ is the proton conductivity (S cm^{-1}), σ_0 is the pre-exponential factor, E_a is the activation energy (kJ mol^{-1}), R is the universal gas constant (8.314 J $mol^{-1}K^{-1}$), and T is the absolute temperature (K).[41] Figure 4b presents the plot of ln σ versus T^{-1} of the NRE-212, recast Nafion, and Nafion−TNT composite membranes measured under 100% RH at different temperatures. It was found that the proton conductivity value of all membranes increased with increasing temperature. The activation energy calculated from the slope of the ln σ versus T^{-1} plot of Nafion−TNT-1.0, Nafion−TNT-1.5, and Nafion−TNT-2.0 membranes was found to be 7.82, 7.10, and 7.99 kJ mol^{-1}, respectively. The activation energy of NRE-212 and

Table 2. Distribution of Water State in Various Nafion Composite Membranes

						no. of water per sulfonic acid group (λ)		
samples	water uptake (%)	IEC (mequiv g^{-1})	Q_{endo}[a] (J g^{-1})	freezable bound and free water (%)	bound water (%)	λ[b]	$\lambda_{freezable}$[c]	λ_{bound}[d]
NRE-212	23.74	0.937	59	17.66	6.08	14.08	10.47	3.60
recast Nafion	21.78	0.938	58	17.37	4.41	12.90	10.29	2.61
Nafion−TNT-1.0	29.91	0.924	60	17.96	11.95	17.98	10.80	7.18
Nafion−TNT-1.5	33.72	0.918	65	19.46	14.26	20.41	11.78	8.63
Nafion−TNT-2.0	33.13	0.913	73	21.86	11.27	20.16	13.30	6.86
Nafion−TNP-2.0	33.42	0.907	68	20.36	13.06	20.47	12.48	8.00
Nafion-ZrNT-1.5[e]	31.95	0.913	66	19.76	12.19	19.44	12.02	7.42
Nafion-CeNT-0.5[f]	27.27	0.931	60	17.96	9.31	16.27	10.72	5.55

[a]The endothermic fusion enthalpy of fully hydrated membrane (freezable loosely bound water and free water). [b]The number of total water molecules per sulfonic acid group. [c]The number of freezable loosely bound water and free water molecules per sulfonic acid group. [d]The number of nonfreezing bound water molecules per sulfonic acid group. [e]The selected membrane based on the optimum ZrNT filler. [f]The selected membrane based on the optimum CeNT filler.

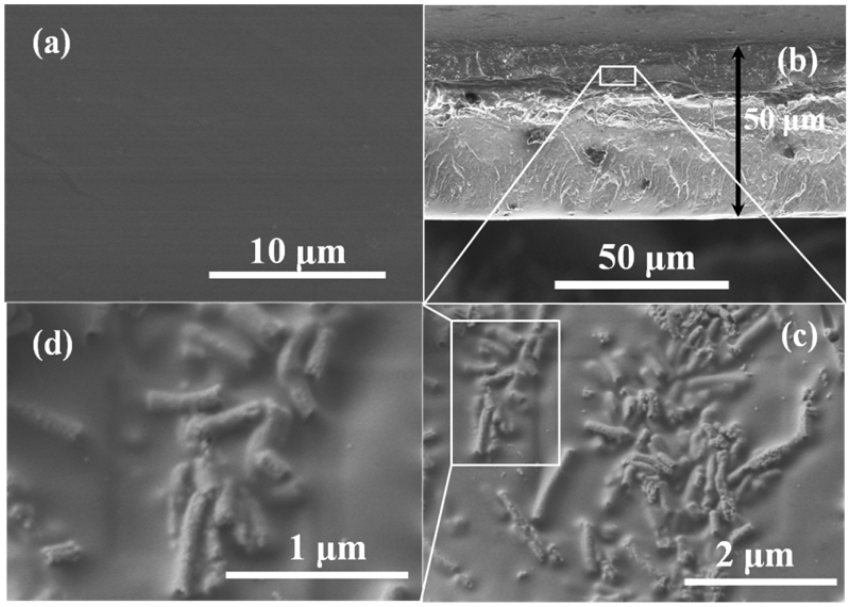

Figure 5. (a) Morphology (top view), (b) cross-section image of Nafion−TNT-1.5 membrane, (c) and (d) high magnification cross-section images of Nafion−TNT-1.5 membrane.

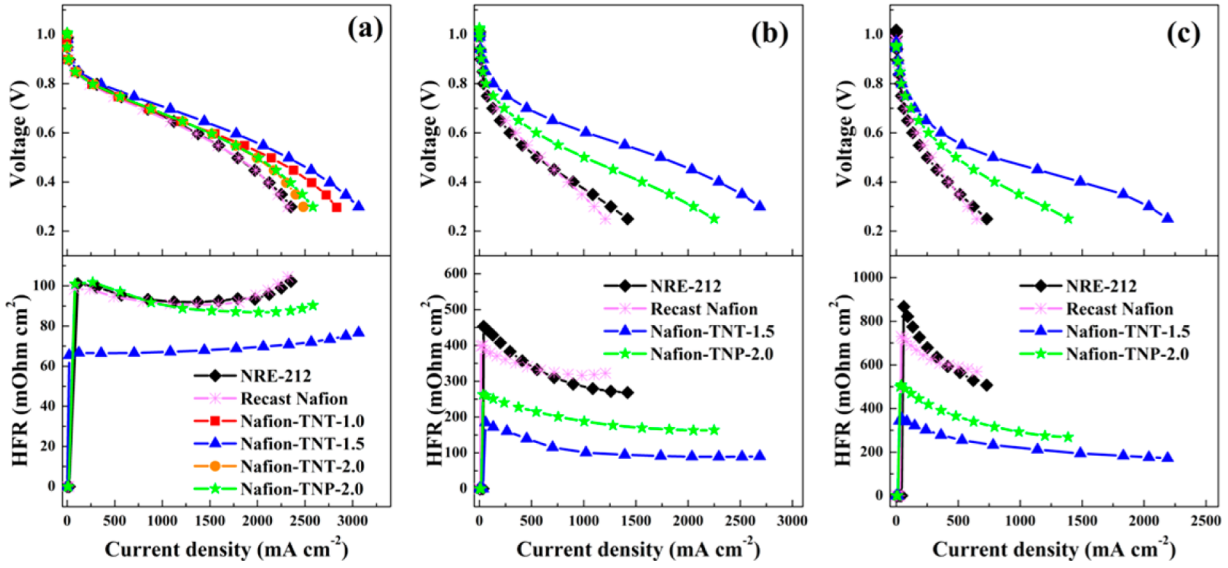

Figure 6. Polarization and high frequency resistance (HFR) plots of NRE-212, recast Nafion, Nafion−TNT, and Nafion−TNP membranes operating under 100% RH at 80 °C (a), under 50% RH at 80 °C (b), and under 18%RH 80 °C (c). The H_2 and O_2 gas flow rates were fixed at 300 SCCM.

recast Nafion membranes was 8.04 and 8.31 kJ mol^{-1}, respectively. The activation energy of Nafion−TNT composite membranes was lower than that of NRE-212 and recast Nafion membranes under 100% RH, indicating that the presence of TNT in the Nafion membrane facilitates the proton migration through the membrane. These activation energy values of the composite membranes are indicative of proton migration through the membranes via the vehicular mechanism.[9] The activation energy values of the composite membranes was similar to the activation energy obtained with that of hybrid Nafion−silica, Nafion-mesoporous zirconium phosphate and Nafion-mesoporous titanium phosphate membranes.[9,41]

Figure 5 illustrates the morphology and cross-section image of the Nafion−TNT-1.5 membrane. It was observed that the surface of the Nafion−TNT membrane was smooth and that TNTs were not present on the surface (Figure 5a), indicating that the TNT may be embedded inside the Nafion membrane. To verify the existence of TNT, the membrane cross-section was investigated by freeze-dry cut, and the cross-section image of the TNT membrane is shown in Figure 5b. The measured average membrane thickness was found to be 50 ± 5 μm. It was observed that the nanotubes were randomly embedded in the Nafion membrane (Figure 5c) and the tubes were completely filled with Nafion ionomer (Figure 5d).

PEFC performance was further evaluated with Nafion−TNT composite membranes and the obtained results were compared with that of recast Nafion and NRE-212 membranes. The catalyst loading on gas diffusion layers was kept identical for all MEAs studies. Figure 6a depicts the polarization plots of recast Nafion, NRE-212, and Nafion−TNT composite membranes at

80 °C under ∼100% RH and ambient pressure. The open circuit voltage (OCV) was roughly 0.99−1.03 V for all membranes, indicating very low H_2 gas permeability from the anode to the cathode through the membrane. To evaluate the effect of TNT on the ohmic resistance of the composite membranes, the current density of the membranes obtained at 0.6 V was compared.[16] The Nafion−TNT-1.0, Nafion−TNT-1.5, and Nafion−TNT-2.0 membranes delivered current density of 1,553, 1,777, and 1,525 mA cm^{-2}, respectively. The NRE-212 and recast Nafion membranes delivered current density of 1,374 and 1,357 mA cm^{-2}, respectively, at the same potential. The current density of Nafion−TNT-1.0, Nafion−TNT-1.5, and Nafion−TNT-2.0 membranes was 1.13, 1.29, and 1.11 times higher, respectively, than that of the NRE-212 membrane, and 1.14, 1.31, and 1.12 times higher than that of the recast Nafion membrane. The higher PEFC performance of the Nafion−TNT composite membrane compared to both NRE-212 and recast Nafion membranes implies that the incorporation of mesoporous TNT in Nafion suppresses the ohmic resistance of the Nafion membrane. To verify the ohmic resistance of the membranes, high frequency resistance (HFR) was then investigated for NRE-212, recast Nafion, and Nafion−TNT-1.5 membranes. Figure 6a presents the HFR of recast Nafion, NRE-212, and Nafion−TNT-1.5 composite membranes at 80 °C under ∼100% RH. It is obvious that the Nafion−TNT-1.5 membrane exhibits substantially lower resistance than the NRE-212 and recast Nafion membranes. The remarkable reduction of ohmic resistance of the Nafion−TNT composite membrane was mainly attributed to its higher proton conductivity. This results from the incorporation of porous tubular hygroscopic TiO_2, which not only functions as a water reservoir but also facilitates water back-diffusion from cathode to the anode through the membrane. Further evidence demonstrating the facile water back-diffusion from cathode to anode through the membrane was investigated by comparing the current density in the polarization plot at low potential (0.3 V, mass transport region). It was found that the current density of Nafion−TNT-1.5 and NRE-212 membranes at 0.3 V under 100% RH at 80 °C was 3,062 and 2,352 mA cm^{-2}, respectively (Figure 6a). The significantly higher current density of Nafion−TNT-1.5 versus NRE-212 membranes implies there is facile water back-diffusion from the cathode to the anode in the composite Nafion−TNT membrane. Considering the high frequency resistance and the current density data at low potential, it could be concluded that the incorporation of mesoporous TNT in the Nafion membrane provided facile proton mobility (higher water self-diffusion coefficient) as well as efficient water back-diffusion from cathode to anode through the membrane (higher current density at low potential) which resulted in significantly improving the PEFCs performance under fully humid conditions.

Figure 6b represents the polarization and HFR plots of Nafion−TNT-1.5 composite membrane compared to results obtained with recast Nafion and NRE-212 membranes under ∼50% RH at 80 °C. The current density of the Nafion−TNT-1.5, NRE-212, and recast Nafion membranes at 0.6 V was 1,021, 293, and 348 mA cm^{-2}. Under 50% RH, the fuel cell performance of the Nafion−TNT-1.5 membrane was substantially higher than that of the recast Nafion and NRE-212 membranes at 80 °C. The current density of the Nafion−TNT-1.5 membrane under 50%RH was ultimately 3.48 times higher than that of the NRE-212 membrane. The superior PEFCs performance of the Nafion−TNT composite membrane operated at 80 °C under 50% RH was apparently due to the lower ohmic resistance of the Nafion−TNT composite membrane compared to NRE-212 and recast Nafion membranes (Figure 6b).

In addition to operation of the composite membranes at 50% and 100% RH at 80 °C, we also evaluated the fuel cell performance of Nafion−TNT-1.5 membrane under 18% RH at 80 °C in comparison with that of recast Nafion and NRE-212 membranes (Figure 6c). The current density of the Nafion−TNT-1.5, NRE-212 and recast Nafion membranes at 0.6 V was 390, 134, and 164 mA cm^{-2}, respectively. The maximum power density of the Nafion−TNT-1.5, NRE-212, and recast Nafion membranes corresponded to 641, 186, and 175 mW cm^{-2} (Supporting Information Figure S4). A **3.4-fold** enhancement in the maximum power density was observed for the Nafion−TNT composite membrane compared with the NRE-212 membrane. The outstanding performance of the Nafion−TNT composite membrane under low RH (18%) was mainly attributed to the extremely low ohmic resistance (Figure 6c) due to the water retention behavior and tubular structure of TiO_2.

To investigate the effects of filler morphology, TiO_2 nanoparticles (TNP, surface area-150 m^2 g^{-1}) were incorporated in Nafion ionomer. The optimum TNP filler loaded in the Nafion ionomer was 2 wt % (Supporting Information Figure S5). Figure 6a compares the polarization and power density plots of Nafion−TNP and Nafion−TNT composite membranes under fully humid conditions (∼100% RH). The Nafion−TNP composite membrane operated at 80 °C (Figure 6a) delivered a current density of 1,520 mA cm^{-2} at 0.6 V. Under fully humid conditions, the Nafion−TNT composite membrane exhibited approximately 1.17 times higher current density than the Nafion−TNP composite membrane. The higher fuel cell performance of Nafion−TNT over Nafion−TNP membranes could be due to the more facile water diffusion in the membrane. To understand water diffusion in these membranes, we measured the water self-diffusion coefficient at 100% RH using PFG NMR. The water self-diffusion coefficient of the Nafion−TNP membrane was 2.02×10^{-9} m^2 s^{-1}. In comparison, the water self-diffusion coefficient of the Nafion−TNT membrane (3.527×10^{-9} m^2 s^{-1}) at 25 °C was 1.75 times higher than that of Nafion−TNP membrane. In addition, the Nafion−TNT membrane also exhibited higher current density at low potential (0.3 V). Furthermore, we also investigated the fuel cell performance of Nafion−TNP composite membrane under 50% and 18% RH at 80 °C (Figure 6b and c). It was found that the Nafion−TNP membrane delivered current densities of 545 and 260 mA cm^{-2} under 50 and 18%RH, respectively (Figure 6b and c). Once again, the Nafion−TNT composite membrane exhibited better PEFCs performance under 50% and 18% RH than the Nafion−TNP composite membrane. In particular, the Nafion−TNT membrane provided higher current density at 0.3 V than Nafion−TNP composite membrane under 18% RH (Figure 6c). The superior performance of the Nafion−TNT over Nafion−TNP membranes in this case was mainly because of the porous tubular morphology, which resulted in substantially lower ohmic resistance (Figure 6a, b, and c). It should be stressed that the porous 1-dimensional tubular morphology provided facile water diffusion (electroosmotic drag and back-diffusion) though the membrane which resulted in low ohmic resistance, leading to high PEFCs performance. It might be expected that, the much higher surface area of TNP (150 m^2

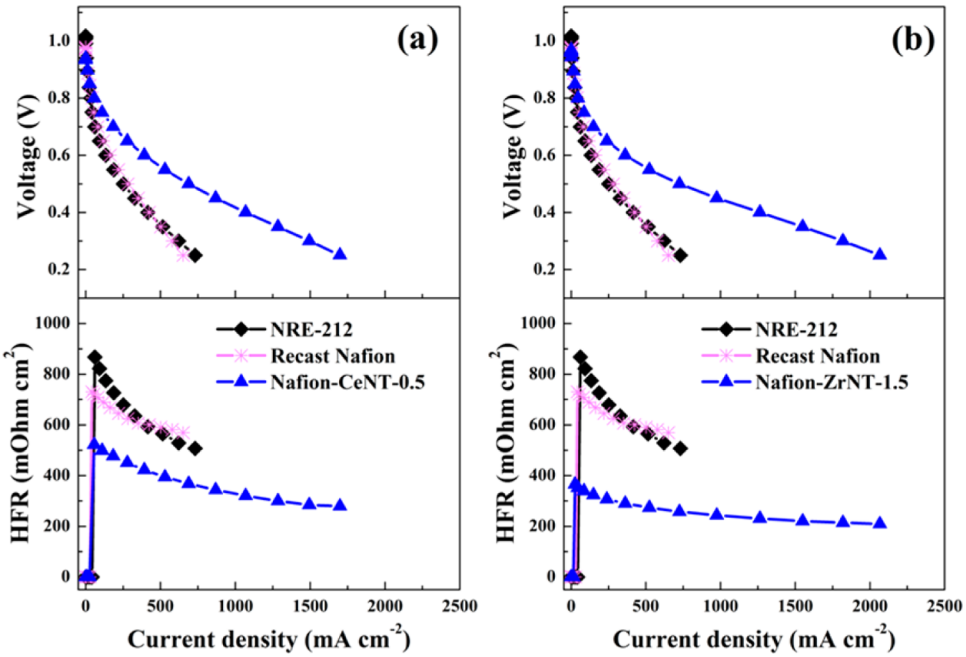

Figure 7. Polarization and high frequency resistance (HFR) plots of NRE-212, recast Nafion, Nafion−CeNT (a), and Nafion−ZrNT (b), membranes operating under 18% RH at 80 °C. The H_2 and O_2 gas flow rates were fixed at 300 SCCM.

g^{-1}), relative to TNT (35 m^2 g^{-1}) should have provided higher water retention to the membrane. However, the smaller size nanoparticles easily aggregated with each other, resulting in poor dispersion in the Nafion membranes. The poorly dispersed TNP led to low water uptake, and moreover, the water retention in the Nafion−TNP membrane was found to be slightly lower than in the Nafion−TNT membrane with a TNT content of 1.5 wt % (Table 2).

To investigate the effect of the tubular morphology of the metal oxide on the substantial improvement of PEFC performance under low RH, mesoporous CeNT and mesoporous ZrNT were utilized to fabricate Nafion composite membranes, and then the PEFC performance of those composite membranes was evaluated at 80 °C under 18%RH. The optimum loading CeNT and ZrNT fillers in Nafion ionomer was found to be 0.5 (Nafion-CeNT-0.5) and 1.5 wt % (Nafion-ZrNT-1.5), respectively (Supporting Information Figures S6 and S7). Figure 7 (a, b) compares the PEFC performance of Nafion-CeNT-0.5 (Figure 7a) and Nafion-ZrNT-1.5 (Figure 7b) with that of NRE-212 and recast Nafion membranes. The Nafion-CeNT-0.5 and Nafion-ZrNT-1.5 membranes provided a maximum power density of 449 and 546 mW cm^{-2}, respectively (Supporting Information Figure S4). The maximum power density of Nafion-CeNT-0.5 and Nafion-ZrNT-1.5 membranes was approximately 2.41 and 2.93 times higher than that of the NRE-212 membrane, respectively. The results of the PEFC performance of Nafion−TNT, Nafion−CeNT, and Nafion−ZrNT composite membranes clearly demonstrate that the porous tubular metal oxide greatly enhanced the fuel cell performance when operated at low RH compared to NRE-212 and recast Nafion membranes.

Membrane degradation is typically due to the formation of H_2O_2 by the permeation of O_2 gas from the cathode through the membrane to the anode.[41] This gas permeability can be directly detected by the reduction of the OCV. Figure 8 presents the preliminary durability studies of Nafion−TNT and NRE-212 membranes for 50 h under 100% RH at 80 °C. The

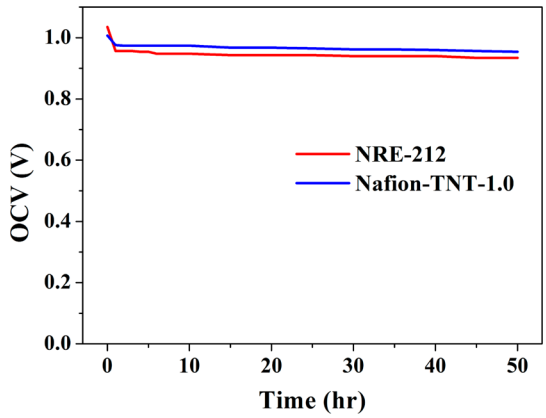

Figure 8. Durability test of Nafion−TNT and NRE-212 membranes under 100%RH at 80 °C. The H_2 and O_2 gases flow rate were fixed at 300 SCCM.

OCV of the Nafion−TNT membrane decreased from 1.007 to 0.954 V after 50 h of operation. The OCV of NRE-212 membrane declined from 1.035 to 0.931 V. The OCV reduction rate of Nafion−TNT-1.0 and NRE-212 membranes was 1.06 and 2.08 mV h^{-1}, respectively. The lower OCV reduction rate of the composite membrane indicates that the TNT were capable of preventing O_2 gas diffusion from the cathode to the anode, which has effect of hindering the generation of H_2O_2 at the anode.[41]

CONCLUSIONS

In this study we successfully incorporated porous hygroscopic TNT, CeNT, and ZrNT in a Nafion membrane, which served as water reservoirs during PEFC operation under low RH. Mesoporous TNT, CeNT, and ZrNT were synthesized by thermal annealing of an electrospun nonwoven web, which was fabricated by a conventional single spinneret electrospinning technique, under an air atmosphere. The morphology of porous

metal oxide nanotubes composed of small particles joined together forming tube wall. Incorporating of tubular TNT, CeNT, and ZrNT fillers into a Nafion membrane resulted in increased water retention capability as well as a higher water diffusion coefficient, which facilitated the enhancement of proton conductivity of the composite membrane under both fully humid and dry conditions. Compared to NRE-212 and Nafion−TNP membranes operated under fully humid conditions (100%RH) at 80 °C, the Nafion−TNT composite membranes exhibited better PEFC performance. Under dry conditions (18% RH, 80 °C), the Nafion−TNT, Nafion−CeNT, and Nafion-ZrNT composite membranes remarkably improved PEFC performance as compared with a commercial membrane. The enhanced performance of fuel cell employing the composite membranes can be attributed to the membrane's excellent water retention capability as well as their facile water diffusion.

■ ASSOCIATED CONTENT

Supporting Information

Additional figures showing fiber diameter, DSC thermograms, PFG NMR spectra, and polarization and power density plots. This material is available free of charge via the Internet at http://pubs.acs.org.

■ AUTHOR INFORMATION

Corresponding Author

*Phone: (+82)-53-785-6413. E-mail: sangarajus@dgist.ac.kr.

Notes

The authors declare no competing financial interest.

■ ACKNOWLEDGMENTS

This work was supported by the DGIST R&D Program of the Ministry of Education, Science and Technology of Korea (14-BD-01).

■ REFERENCES

(1) Devanathan, R. Recent Developments in Proton Exchange Membrane for Fuel Cells. *Energy Environ. Sci.* **2008**, *1*, 101−119.

(2) He, G.; Li, Z.; Li, Y.; Li, Z.; Wu, H.; Yang, X.; Jiang, Z. Zwitterionic Microcapsules as Water Reservoirs and Proton Carriers within a Nafion Membrane To Confer High Proton Conductivity under Low Humidity. *ACS Appl. Mater. Interfaces* **2014**, *6*, 5362−5366.

(3) Li, Z.; He, G.; Zhang, B.; Cao, Y.; Wu, H.; Jiang, Z.; Tiantian, Z. Enhanced Proton Conductivity of Nafion Hybrid Membrane under Different Humidities by Incorporating Metal−Organic Frameworks With High Phytic Acid Loading. *ACS Appl. Mater. Interfaces* **2014**, *6*, 9799−9807.

(4) Kreuer, K. D. Proton Conductivity: Materials and Applications. *Chem. Mater.* **1996**, *8*, 610−641.

(5) Muriithi, B.; Loy, D. A. Processing, Morphology, and Water Uptake of Nafion/Ex situ Stober Silica Nanocomposite Membranes as a Function of Particle Size. *ACS Appl. Mater. Interfaces* **2012**, *4*, 6766−6773.

(6) Amiinu, I. S.; Liang, X.; Tu, Z.; Zhang, H.; Feng, J.; Wan, Z.; Pan, M. Anhydrous Proton Conducting Materials Based on Sulfonated Dimethylphenethylchlorosilane Grafted Mesoporous Silica/Ionic Liquid Compsite. *ACS Appl. Mater. Interfaces* **2013**, *5*, 11535−11543.

(7) Zeng, J.; He, B.; Lamb, K.; Marco, R. D.; Shen, P. K.; Jiang, S. P. Anhydrous Phosphoric Acid Functionalized Sintered Mesoporous Silica Nanocomposite Proton Exchange Membrane for Fuel Cells. *ACS Appl. Mater. Interfaces* **2013**, *5*, 11240−11248.

(8) Xu, K.; Chanthad, C.; Gadinski, M. R.; Hickner, M. A.; Wang, Q. Acid-Functionalized Polysilsesquioxane-Nafion Composite Membranes with High Proton Conductivity and Enhanced Selectivity. *ACS Appl. Mater. Interfaces* **2009**, *1*, 2573−2579.

(9) Pereira, F.; Valle, K.; Belleville, P.; Morin, A.; Lambert, S.; Sanchez, C. Advanced Mesostructured Hybrid Silica-Nafion Membranes for High Performance PEM Fuel Cell. *Chem. Mater.* **2008**, *20*, 1710−1718.

(10) Lee, H. J.; Kim, J. H.; Won, J. H.; Lim, J. M.; Hong, Y. T.; Lee, S. Y. Highly Flexible, Proton Conductive Silicate Electrolyte for Medium-Temperature/Low-Humidity Proton Exchange Membrane Fuel Cells. *ACS Appl. Mater. Interfaces* **2013**, *5*, 5034−5043.

(11) Adjemian, K. T.; Dominey, R.; Krishnan, L.; Ota, H.; Majsztrik, P.; Zhang, T.; Mann, J.; Kriby, B.; Gatto, L.; Simpson, M. V.; Leahy, J.; Srinivasan, S.; Benziger, J. B.; Bocarsly, A. B. Function and Characterization of Metal Oxide−Nafion Composite Membranes for Elevated-Temperature H_2/O_2 PEM Fuel Cells. *Chem. Mater.* **2006**, *18*, 2238−2248.

(12) Jalani, N. H.; Dunn, K.; Datta, R. Synthesis and Characterization of Nafion−MO_2 (M = Zr, Si, Ti) Nanocomposite Membranes for Higher Temperature PEM Fuel Cells. *Electrochim. Acta* **2005**, *51*, 553−560.

(13) Mohammadi, Gh.; Jahanshahi, M.; Rahimpour, A. Fabrication and Evaluation of Nafion Nanocompoiste Membrane Based on ZrO_2−TiO_2 Binary Nanoparticles as Fuel Cell MEA. *Int. J. Hydrogen Energy* **2013**, *38*, 9387−9394.

(14) Watanabe, M.; Uchida, H.; Seki, Y.; Emori, M.; Stonehart, P. Self-Humidifying Polymer Electrolyte Membranes for Fuel Cells. *J. Electrochem. Soc.* **1996**, *143*, 3847−3852.

(15) Patil, Y.; Sambandam, S.; Ramani, V.; Mauritz, K. Perfluorinated Polymer Electrolyte Hybridized with In Situ Grown Titania Quasi-Networks. *ACS Appl. Mater. Interfaces* **2013**, *5*, 42−48.

(16) Matos, B. R.; Santiago, E. I.; Fonseca, F. C.; Linardi, M.; Lavayen, V.; Lacerda, R. G.; Ladeira, L. O.; Ferlauto, A. S. Nafion−Titanate Nanotube Composite Membranes for PEMFC Operating at High Temperature. *J. Electrochem. Soc.* **2007**, *154*, B1358−B1361.

(17) Jun, Y.; Zarrin, H.; Fowler, M.; Chen, Z. Functionalized Titania Nanotube Composite Membrane for High Temperature Proton Exchange membrane Fuel Cells. *Int. J. Hydrogen Energy* **2011**, *36*, 6073−6081.

(18) Wu, X.; Scott, K. A PFSA Composite Membrane with Sulfonic Acid Functionalized TiO_2 Nanotubes for Polymer Electrolyte Fuel Cells and Water Electrolyzes. *Fuel Cells* **2013**, *6*, 1138−1145.

(19) Chalkova, E.; Pague, M. B.; Fedkin, M. V.; Wesolowski, D. J.; Lvov, S. N. Nafion/TiO_2 Proton Conductive Composite Membranes for PEMFC Operating at Elevated Temperature and Reduced Relative Humidity. *J. Electrochem. Soc.* **2005**, *152*, A1035−A1040.

(20) Sacca, A.; Carbone, A.; Passalacqua, E.; Epifanio, A. D.; Licoccia, S.; Traversa, E.; Sala, E.; Traini, F.; Ornelas, R. Nafion−TiO_2 Hybrid Membranes for Medium Temperature Polymer Electrolyte Fuel Cells (PEFCs). *J. Power Sources* **2005**, *152*, 16−21.

(21) Noto, V. D.; Bettiol, M.; Bassetto, F.; Boaretto, N.; Negro, E.; Lavina, S.; Bertasi, F. Hybrid Inorganic−Organic Nanocomposite Polymer Electrolytes Based on Nafion and Fluorinated TiO_2 for PEMFCs. *Int. J. Hydrogen Energy* **2012**, *37*, 6169−6181.

(22) Santiago, E. I.; Isidoro, R. A.; Dresch, M. A.; Matos, B. R.; Linardi, M.; Fonseca, F. C. Nafion−TiO_2 Hybrid Electrolytes for Stable Operation of PEM Fuel Cells at High Temperature. *Electrochim. Acta* **2009**, *54*, 4111−4117.

(23) Amjadi, M.; Rowshanzamir, S.; Peighambardoust, S. J.; Hosseini, M. G.; Eikani, M. H. Investigation of Physical Properties and Cell Performance of Nafion/TiO_2 Nanocomposite Membranes for High Temperature PEM Fuel Cells. *Int. J. Hydrogen Energy* **2010**, *35*, 9252−9260.

(24) Zhengbang, W.; Haolin, T.; Mu, P. Self-Assembly of Durable Nafion/TiO_2 Nanowire Electrolyte Membranes for Elevated-temperature PEM Fuel Cells. *J. Membr. Sci.* **2011**, *369*, 250−257.

(25) Abbaraju, R. R.; Dasgupta, N.; Virkar, A. V. Composite Nafion Membrane Containing Nanosize TiO_2/SnO_2 for Proton Exchange Membrane Fuel Cells. *J. Electrochem. Soc.* **2008**, *155*, B1307−B1313.

(26) Sacca, A.; Gatto, I.; Carbone, A.; Pedicini, R.; Passalacqua, E. ZrO_2–Nafion Composite Membrane for Polymer Electrolyte Fuel Cells (PEFCs) at Intermediate Temperature. *J. Power Sources* **2006**, *163*, 47–51.
(27) D'Epifanio, A.; Navarra, M. A.; Weise, F. C.; Mecheri, B.; Farrington, J.; Licoccia, S.; Greenbaum, S. Composite Nafion/Sulfated Zirconia Membranes: Effect of the Filler Surface Properties on Proton Transport Characteristics. *Chem. Mater.* **2010**, *22*, 813–821.
(28) Lu, S.; Wang, D.; Jiang, S. P.; Xiang, Y.; Lu, J.; Zeng, J. HPW/MCM-41 Phosphotungstic Acid/Mesoporous Silica Composites as Novel Proton-Exchange Membranes for Elevated-Temperature Fuel Cells. *Adv. Mater.* **2010**, *22*, 971–976.
(29) Chen, Z.; Holmberg, B.; Li, W.; Wang, X.; Deng, W.; Munoz, R.; Yan, Y. Nafion/Zeolite Nanocomposite Membrane by In Situ Crystallization for a Direct Methanol Fuel Cell. *Chem. Mater.* **2006**, *18*, 5669–5675.
(30) Kasuga, T.; Hiramatsu, M.; Hoson, A.; Sekino, T.; Niihara, K. Titania Nanotubes Prepared by Chemical Processing. *Adv. Mater.* **1999**, *11*, 1307–1311.
(31) Macak, J. M.; Tsuchiya, H.; Schmuki, P. High-Aspect-Ratio TiO_2 Nanotubes by Anodization of Titanium. *Angew. Chem., Int. Ed.* **2005**, *44*, 2100–2102.
(32) Li, D.; Xia, Y. Direct Fabrication of Composite and Ceramic Hollow Nanofibers by Electrospinning. *Nano Lett.* **2004**, *4*, 933–938.
(33) Lu, B.; Zhu, C.; Zhang, Z.; Lan, W.; Xie, E. Preparation of Highly Porous TiO_2 Nanotube and their Catalytic Applications. *J. Mater. Chem.* **2012**, *22*, 1375–1379.
(34) Ketpang, K.; Kim, M.; Kim, S.; Shanmugam, S. High Performance Catalyst for Electrochemical Hydrogen Evolution Reaction Based on SiO_2/WO_{3-x} Nanofacets. *Int. J. Hydrogen Energy* **2013**, *38*, 9732–9740.
(35) Yang, A. C. C.; Narimani, R.; Zhang, Z.; Frisken, B. J.; Holdcroft, S. Controlling Crystallinity in Graft Ionomers, and Its Effect on Morphology, Water Sorption, and Proton Conductivity of Graft Ionomer Membrane. *Chem. Mater.* **2013**, *25*, 1935–1946.
(36) Kim, T.; Choi, Y. W.; Kim, C. S.; Yang, T. H.; Kim, M. N. Sulfonated Poly(Arylene Ether Sulfone) Membrane Containing Sulfated Zirconia for High Temperature Operation of PEMFCs. *J. Mater. Chem.* **2011**, *21*, 7612–7621.
(37) Sing, K. S. W.; Everett, D. H.; Haul, R. A. W.; Moscou, L.; Pierotti, R. A.; Rouquerol, J.; Siemieniewska, T. Reporting Physisorption Data for Gas/Solid Systems with Special Reference to the Determination of Surface Area and Porosity. *Pure Appl. Chem.* **1985**, *57*, 603–619.
(38) Vichi, F. M.; Tejedor, M. I. T.; Anderson, M. A. Effect of Pore–Wall Chemistry on Proton Conductivity in Mesoporous Titanium Dioxide. *Chem. Mater.* **2000**, *12*, 1762–1770.
(39) Chen, X.; Unruh, K. M.; Ni, C.; Ali, B.; Sun, Z.; Lu, Q.; Deitzel, J.; Xiao, Q. Fabrication, Formation Mechanism, and Magnetic Properties of Metal Oxide Nanotubes via Electrospining and Thermal Treatment. *J. Phys. Chem. C* **2011**, *115*, 373–378.
(40) Sahu, A. K.; Bhat, S. D.; Pitchumani, S.; Sridhar, P.; Vimalan, V.; George, C.; Chandrakumar, N.; Shukla, A. K. Novel Organic–Inorganic Composite Polymer–Electrolyte Membranes for DMFCs. *J. Membr. Sci.* **2009**, *345*, 305–314.
(41) Ohma, A.; Yamamoto, S.; Shinohara, K. Membrane Degradation Mechanism during Open-Circuit Voltage Hold Test. *J. Power Sources* **2008**, *182*, 39–47.